PHYSICAL REVIEW B **76**, 134515 (2007)

1/*f* flux flow noise due to a coexistence of qualitatively different vortex states

D. Babić,[1,*] J. Bentner,[2,†] C. Sürgers,[3] and C. Strunk[2]
[1]*Department of Physics, Faculty of Science, University of Zagreb, Bijenička 32, HR-10000 Zagreb, Croatia*
[2]*Institute for Experimental and Applied Physics, University of Regensburg, D-93025 Regensburg, Germany*
[3]*Physikalisches Institut and DFG Center for Functional Nanostructures (CFN), Universität Karlsruhe, D-76128 Karlsruhe, Germany*
(Received 2 July 2007; revised manuscript received 24 August 2007; published 25 October 2007)

We investigate the vortex-motion voltage noise in a hybrid structure consisting of a weak-pinning amorphous $Nb_{0.7}Ge_{0.3}$ microbridge on top of which a strong-pinning, longitudinal Nb line with a narrow interruption in the middle is added. The Nb part enforces a branching of the applied current, causing a modulation of the current density within the $Nb_{0.7}Ge_{0.3}$, where vortex motion induces a voltage. When the $Nb_{0.7}Ge_{0.3}$ is sufficiently dissipative, the modulation is strong and the vortex dynamics is spatially dependent. Under these circumstances, the distribution function for normal excitations in vortex cores varies considerably over the sample, which results in a coexistence of distinct vortex states spreading from nearly equilibrium to strongly nonequilibrium ones. This leads to a range of characteristic times for the voltage fluctuations and, consequently, to the frequency (f) dependence of the noise being of $1/f$ type. The noise originates in the fluctuations of the vortex-core size around the average set by the nonequilibrium effects in vortex motion.

DOI: 10.1103/PhysRevB.76.134515 PACS number(s): 74.25.Qt, 74.40.+k, 74.78.Db

I. INTRODUCTION

Every observable is noisy, i.e., it fluctuates around its average. In most experiments, one measures a time-averaged signal to extract the mean value which, however, does not contain full information on the physics involved. Namely, the noise is not a nuisance but reflects effects that are often hindered by averaging. For instance, fluctuations of the electric current I in mesoscopic normal conductors reveal not only the charge of the carriers but also interactions they undergo.[1] Electronic conduction is not the only transport phenomenon where a I or a voltage V is applied and the noise in the response is measured. As a relevant historical example, we stress the pioneering work of van Ooijen and van Gurp,[2] who tackled the possibility that supercurrent vortices could exhibit shot noise, a fluctuation characteristic of electrons. The symmetry arises from the discretenesses of the magnetic flux ϕ_0 carried by the vortex and the electron charge e, i.e., $eV \leftrightarrow \phi_0 I$.

In our study[3] on the vortex-motion noise in weak-pinning amorphous $Nb_{0.7}Ge_{0.3}$ (throughout the paper denoted as a-NbGe) microbridges, in a single experiment we identified three types of noise commonly associated with conducting electrons. The voltage-noise power S_V at the average voltage $\langle V\rangle = 0$ matched the Johnson-Nyquist noise $4k_BT(d\langle V\rangle/dI)$, T being temperature and k_B the Boltzmann constant.[4] In the dynamic excess noise $\Sigma_V = S_V - 4k_BT(d\langle V\rangle/dI)$, we observed a hallmark of shot noise $\sim 2\phi_0\langle V\rangle$ when vortices hopped more or less individually from one pinning site to another. The third and perhaps the most intriguing result of this experiment was the appearance of fluctuations for a linear $\langle V(I)\rangle$ related to a pinning-free, viscous flow of vortices, the properties of which were the same as in equilibrium. We found $\Sigma_V \propto (1 - B/B_{c2})^2\langle V\rangle^2/f^\gamma$, where B was the applied magnetic field, B_{c2} the upper critical magnetic field, and $\gamma = 1.5 \pm 0.1$. $\Sigma_V \propto \langle V\rangle^2$ fitted into the class of resistance fluctuations, typical of electron transport,[5–9] whereas $\Sigma_V \propto (1 - B/B_{c2})^2$ was consistent with vortex-core-size fluctuations (VCSF's) as inferred from the Larkin-Ovchinnikov (LO) theory of Ohmic flux-flow dissipation.[10] The softness of the vortex-core boundary in a-NbGe, as a precursor for the VCSF's, was later confirmed by detailed $\langle V(I)\rangle$ measurements.[11,12] However, $\Sigma_V \propto 1/f^\gamma$ was not clarified with the same certainty. Actually, γ was intermediate between 1 and 2, the latter value corresponding to the high-frequency tail of a Debye-Lorentz (DL) spectrum.

$1/f$ type of vortex-motion noise was also observed by other authors, both in the presence[13] and absence[14] of pinning. As in Ref. 3, the reasoning in explaining the $1/f$ shape of Σ_V relied on a standard model of a statistically weighted superposition of DL spectra over a range of characteristic times τ for the fluctuations,[15,16] but this was substantiated by implicit assumptions only. Similarly as in numerous other studies on $1/f$ noise, the reason for the range of τ in a macroscopically homogeneous motion of "particles", in our case vortices, poses a nontrivial problem. Its understanding requires an insight into the structural and/or thermodynamic properties that influence the vortex matter, which cannot be acquired by experiments on vortex transport only. This restriction becomes less serious if the experimental design makes it possible to suppress the relevance of parameters beyond the reach of transport measurements, which is the idea employed in this paper. Generally, a range of τ implies an inhomogeneity of processes that cause fluctuations, which can be a consequence of an intrinsic disorder or perhaps of a deliberate implementation of a spatially nonuniform dynamics. The latter, appealing situation could, for vortices, be realized by affecting their fundamental properties locally. In strongly nonequilibrium vortex transport, at a high current density J, the distribution function for normal excitations changes sufficiently to alter vortex-core properties.[10,17] An inhomogeneity could be produced by introducing a strong variation of J over the sample, so that different vortex states—determined by the local properties of the distribution function—are present simultaneously. Since VCSF's accompany the nonequilibrium changes of vortices naturally, the

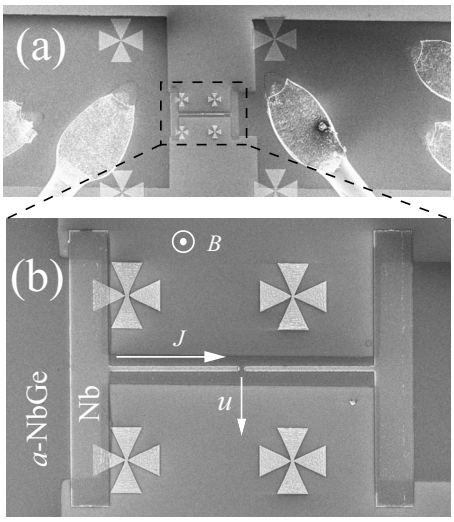

FIG. 1. Photographs of sample G (the *a*-NbGe layout for samples L and P is identical). (a) The whole structure with the bonds for four-point measurements. (b) Expanded view of the microbridge area, with the designation of the materials. The direction of B and the average directions of J and vortex velocity u are indicated.

spread in τ should be related to different relaxation processes for qualitatively distinct vortex cores.

We pursue the above physical picture by fabricating a hybrid *a*-NbGe/Nb sample shown in Fig. 1. With this geometrical design and the materials used, we obtain a system appropriate for imposing a spatially varying dynamics to a small number of vortices, which, in turn, leads to a high sensitivity of the measured V to local conditions. The weak-pinning *a*-NbGe material in the form of a microbridge serves as a medium for vortex motion, so the main task is to produce a modulation of J therein. This is accomplished by making use of a strong-pinning Nb structure—a longitudinal line with a narrow interruption in the middle—patterned on top of the *a*-NbGe microbridge. The presence of the Nb addition results in a branching of the applied current coming from the *a*-NbGe contact pads into the *a*-NbGe/Nb microbridge area. The branching produces a modulation of J within the *a*-NbGe since a part of the current flows through the Nb and returns to the *a*-NbGe at the interruption. When the modulation of J is pronounced, the noise spectra are proportional to $1/f^{\nu}$—with ν equal to or slightly larger than unity—which has a direct link to a strong inhomogeneity of vortex states over the microbridge. The $\langle V\rangle$, T, and B properties of the noise magnitude can be explained consistently by the VCSF's model in combination with the current knowledge on strongly nonequilibrium vortex dynamics,[10,11,17,18] without any obvious necessity for considering material-dependent disorder or particularities of thermodynamic vortex configurations.

II. EXPERIMENT

The samples were produced by combining electron-beam lithography and magnetron sputtering in a two-stage lift-off procedure with polymethyl metacrylate as a resist. *a*-NbGe was deposited onto an oxidized Si substrate, forming several identical microbridges ($l=50$ μm long, $w=5$ μm wide, and 20 nm thick) between large contact pads. This was followed by a second lithography step and a deposition of Nb on top of selected microbridges. The most extensively studied sample (sample G), shown in Fig. 1, comprised a "gate" for vortex motion. The Nb addition was an 800 nm wide and 75 nm thick line centered along the microbridge main axis, interrupted by an ~ 1 μm wide opening in the middle and expanded to an area of ~ 2500 μm^2 on each pad. Another hybrid sample (sample L), similar to sample G but with a continuous Nb line, and a plain microbridge (sample P) with no Nb additions were also prepared to better comprehend the properties of sample G through a comparison.

Electrical contacts to the samples were made by ultrasonic bonding of Al wires onto the large *a*-NbGe contact pads in a standard four-point geometry. The voltage probes were placed as close as possible to the microbridges. Although arrangements with long and narrow leads from the measured area to the bonds are feasible for *a*-NbGe,[19] microbridges are more suitable for experiments on vortex-motion noise in small samples. Namely, in the former case, the resistance of the *a*-NbGe part of the voltage lines may reach the kilohms range, which not only enhances the background Johnson-Nyquist noise but also reduces the useful bandwidth by lowering the high-frequency cutoff to the signal due to the RC filtering. The choice of Nb, which remained dissipationless over the (I,T,B) range of our measurements, as a current-modifying structure resulted in a suppression of parasite heating.

As shown in Fig. 1, B was perpendicular to the film plane, a current was passed along the microbridge, and vortices, hence, traversed the sample perpendicularly to the long microbridge axis. Around 6%–8% of the voltage in the Ohmic regime was induced in the pads, and even less when the dissipation originated in nonlinear electric field (E) vs J curves.[11] Throughout the paper, we present $\langle V\rangle$ and Σ_V referring to the whole area between the voltage probes, which is justified by the voltage drop over the pads being not only small but also nearly the same for the three samples. The exact geometry is, however, taken into account in extracting the resistivity ρ of the *a*-NbGe, important in determining its superconductivity parameters accurately. Measurements were carried out in a ^{3}He cryostat equipped with rf-filtered leads. A cross-correlation technique[1] was used for noise measurements. In short, the outputs of two amplifiers that process the same signal from the voltage probes are cross correlated, which cancels out the (uncorrelated) internal noise of the amplifiers. The cross correlation is performed by a spectrum analyzer which calculates time-averaged $S_V(f)$ spectra in a selected frequency window (f_1,f_2). In our measurements, at different fixed $\langle V\rangle$ (set by constant I, T, and B), we recorded $S_V(f)$ for $f_1=8$ kHz and $f_2=11.2$ kHz. $\Delta f=f_2-f_1$ was small enough to provide high resolution, because the spectra were free of background noise peaks that could not be eliminated by the cross correlation, and, at the same time, sufficiently large [1/3 of $\bar{f}=(f_2+f_1)/2=9.6$ kHz] to permit tracking of changes in the shape $S_V(f)$. The calibration of the

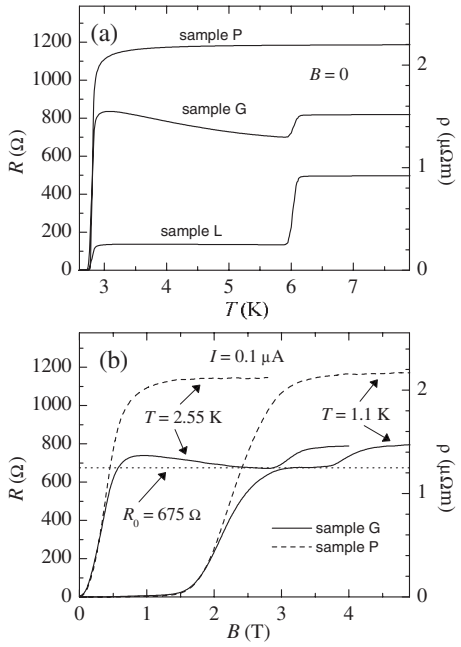

FIG. 2. (a) $R(T,0)$ of the samples showing $T_c=2.8$ K and $T_c^{\mathrm{Nb}} \approx 6$ K. (b) $R(T=\mathrm{const},B)$ of sample G (solid lines) and sample P (dashed lines) at $T=1.1$ K ($B_{c2}=3.1$ T, $B_{c2}^{\mathrm{Nb}} \approx 4.3$ T) and $T=2.55$ K ($B_{c2}=0.7$ T, $B_{c2}^{\mathrm{Nb}} \approx 3.3$ T). The dotted line indicates $R_0=675\ \Omega$. In both (a) and (b), the right-hand scale displays the $\rho(T,B)$.

noise-measurement setup against the Johnson-Nyquist noise was performed in the fully normal state of the samples, above the superconducting transition temperature T_c^{Nb} of the Nb structure. In the calibration, we found no voltage dependence of S_V, thus the voltage-dependent noise originates in the mixed-state phenomena.

III. AVERAGE DISSIPATION

From the low-current (0.1 μA) Ohmic resistance $R(T,B)$ of sample P, we characterize the a-NbGe material, while these results for samples G and L are used for inferring the effects of adding Nb on top of it. These findings are utilized in interpreting the $\langle V(I)\rangle$ curves, which is necessary for dealing with the related Σ_V. Henceforth, J refers explicitly to the current density in a-NbGe, and the brackets denote not only averages in time but also with respect to the spatial modulation of J, if present.

A. Sample characterization

In Fig. 2(a), we show the $R(T,0)$ of the samples (left-hand scale), with the right-hand scale referring to the $\rho(T,0)$ of the same shape as the resistance of sample P. The superconducting transitions at T_c of the a-NbGe in samples G and L agree with that of sample P within a few millikelvins. A set of the $\rho(T,B)$ results is used for finding the superconductivity parameters of the a-NbGe (Refs. 3, 11, and 19): $T_c=2.80$ K, the extrapolated normal-state resistivity $\rho_n(T\to 0)=2.15\ \mu\Omega$ m, $-(dB_{c2}/dT)_{T=T_c}=2.8$ T/K, the Ginzburg-Landau parameters $\kappa=87$, $\xi(0)=6.5$ nm, and $\lambda(0)=0.92\ \mu$m. In our experiment, we concentrate on two characteristic temperatures, well below (1.1 K) and close to (2.55 K) T_c, which have been shown to reveal the basic mechanisms of vortex-motion dissipation in a-NbGe without[11] and with[12,20] a weak modulation of J. The B_{c2} values are found as described in Refs. 3 and 11, being 3.1 T at 1.1 K and 0.7 T at 2.55 K.

The upper step in the $R(T,0)$ of samples G and L, at $T \approx 6$ K, represents the superconducting transition of the Nb at T_c^{Nb}. Similarly, the high-B step in the $R(T=\mathrm{const},B)$ of sample G in Fig. 2(b) (solid lines) arises from the transition at the upper critical magnetic field B_{c2}^{Nb} of the Nb, which exceeds the B_{c2} considerably. The values of T_c^{Nb} and B_{c2}^{Nb} are consistent with the Nb material being disordered.[21] Noteworthy, critical current density in disordered Nb well below T_c^{Nb} and B_{c2}^{Nb} is of the order of 10^4 MA/m^2,[21] which is at least an order of magnitude higher than the estimated maximum current density through the Nb in any measurement of this experiment.

The same T_c in the three samples, the well defined steps at $R(T_c^{\mathrm{Nb}},0)$ and $R(T=\mathrm{const},B_{c2}^{\mathrm{Nb}})$ for samples G and L, and the overall smoothness of the $R(T,B)$ are in favor of a conclusion that the bulk superconductivity in both superconductors is well defined. This, however, does not apply to their interface. In sample L, for $T_c<T<T_c^{\mathrm{Nb}}$, the measured resistance is $\sim 50\ \Omega$ higher than expected for the area of the pads between the voltage probes and also weakly exhibits a $dR/dT<0$. If the a-NbGe/Nb interface were perfect, this would not be the case: the current would flow over the Nb without dissipation and only R from the pads, showing a weak $dR/dT>0$ of the a-NbGe, would be measured. Thus, during the deposition of the Nb, a normal material formed at the interface of a-NbGe and Nb. Consequently, when $\rho=0$, the current coming from the pads simply continues through the a-NbGe, and therefore the superconducting transition at T_c in samples L and G. On the other hand, when $\rho>0$, the current splits into two branches: one continues through the a-NbGe, whereas the other one passes through the Nb line. There are arguments in support of the interface being weakly resistive. The measured value of 50 Ω implies that at least 95% of the current is carried by the Nb, which is possible only if the interface resistance R_{int} is small. Moreover, the $dR/dT<0$ can be explained only by a continuous (along the entire Nb line) branching of the current density, not the current, so the relationship between ρ and R_{int} sets the effective volume that the current through the a-NbGe explores. This interplay of ρ and R_{int} determines the exact shape of the $R(T,B)$, which does not necessarily follow that of ρ since J is nonuniform and may even produce an opposite dependence of the total resistance on T (and B, see below) as a consequence of the variable effective volume.

The above behavior is much more pronounced in sample G, which is clearly seen in Figs. 2(a) and 2(b), because the current at the interruption must flow entirely through the a-NbGe and the modulation of J is, therefore, stronger. Since R in Fig. 2(b) is Ohmic, as deduced from the $\langle V(I)\rangle$ curves, the relationship between ρ and R_{int} determines its shape over the whole B range. When ρ is low, most of the current flows

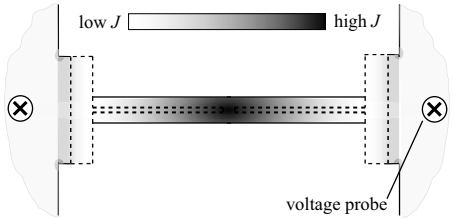

FIG. 3. A schematic representation of J in sample G (not to scale) when the a-NbGe is sufficiently dissipative. The magnitude of J corresponds qualitatively to the gray scale shown.

through the a-NbGe and the dissipations in samples G and P nearly coincide. As ρ increases, more current is taken away by Nb and the resistance of sample G drops below that of sample P. In order to explain the nonmonotonic $R(T,B)$ of sample G quantitatively, one would have to perform a detailed numerical simulation involving ρ, R_{int}, and the consequent coordinate dependence of J, but this is not crucial. It suffices to conclude that when the a-NbGe is dissipative enough, the current branches considerably, and in sample G, a strong modulation of J appears because of the geometrical arrangement, as presented schematically in Fig. 3.

The magnitude of J is depicted by the indicated gray scale, the Nb structure is outlined by the dashed line, and the voltage probes on the contact pads are shown by the encircled crosses. In the pads, the J is low, then it increases in the narrower region until the Nb area where the branching starts is reached, and within the microbridge it is highly modulated. This qualitative picture is in agreement with the fact that the resistance R_0=675 Ω [dashed line in Fig. 2(b)] corresponding to the a-NbGe being normal is much higher than ~100 Ω expected if only the pads and the interruption area were contributing. Therefore, J extends inhomogeneously over the whole area between the contact pads.

The $R(T,0)$ of sample L is consistent with a low R_{int}, which implicitly (e.g., because of the same T_c^{Nb}) suggests the same for sample G. This conclusion is supported by results for a sample of the same geometry but with a highly resistive interface,[22] where the $R(T,B)$ basically follows that of sample P but still shows the features found for sample G, although they are barely observable. The presence of a weakly resistive normal interface is, in fact, an advantage rather than an obstacle for investigating the physics depicted in the Introduction. First, it decouples vortices in the two superconductors effectively, so the properties of those in the a-NbGe are the same as in a plain microbridge. Second, it enhances the current branching as a process continuous along the microbridge, thus giving rise to a strong inhomogeneity of J. Third, it contributes to the total voltage weakly enough to be treated as a small background of no significant influence on the physical mechanisms under consideration.

B. Current-voltage characteristics

In the main panels of Fig. 4, we plot the $\langle V(I)\rangle$ of sample G (solid lines) measured at the same temperatures as in Fig. 2(b), i.e., (a) T=1.1 K and (b) T=2.55 K, and for roughly the same $B<B_{c2}$ ranges. Qualitatively, the $\langle V(I)\rangle$ resembles that

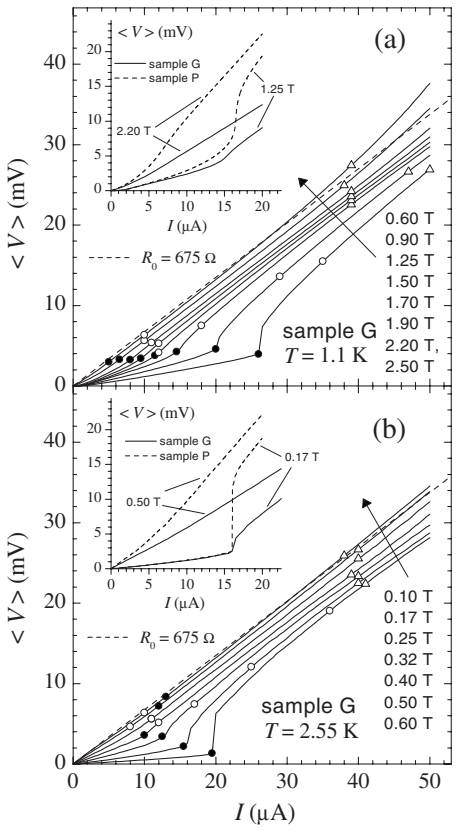

FIG. 4. $\langle V(I)\rangle$ of sample G (solid lines), with B increasing as shown by the arrows, at (a) T=1.1 K and (b) T=2.55 K. The dashed lines represent R_0=675 Ω. The solid circles mark $\langle V_i(I_i)\rangle$ as defined in the text, the open circles the appearance of $\Sigma_V \propto f^{-\nu}$ with ν=1, and the open diamonds the points beyond which $\nu>1$. Insets to (a) and (b): A comparison of selected $\langle V(I)\rangle$ of samples G and P for strongly and weakly nonlinear dependences, with T being the same as in the corresponding main panel and B as indicated.

of a-NbGe in the presence of a homogeneous[11] or a weakly modulated[12,20] J, changing from a strongly nonlinear to a smooth behavior as B increases. In the insets, we compare selected $\langle V(I)\rangle$ of sample G (solid lines) and sample P (dashed lines). Similarly as in Fig. 2(b), the two $\langle V(I)\rangle$ match relatively well at low $\langle V\rangle$, but this does not continue as $\langle V\rangle$ increases. The lower $\langle V(I)\rangle$ of sample G again signifies a considerable current branching in the regime where the a-NbGe is sufficiently dissipative, and, furthermore, the difference in the shape of the $\langle V(I)\rangle$ for the two samples at high $\langle V\rangle$ is reminiscent of a strong modulation of J in sample G. As before, a detailed description of the $\langle V(I)\rangle$ of sample G requires a numerical simulation, complicated further by a necessity to take into account the local nonlinear $E(J)$ response. However, since at the opening the current must flow through the a-NbGe fully, the sketch in Fig. 3 should still be viable and can be used in interpreting the $\langle V(I)\rangle$.

The influence of pinning on the $\langle V(I)\rangle$ in Fig. 4 is marginal, as a-NbGe is a weak-pinning material[3,11,12,20] and the nonlinearities are related mainly to dynamic changes of vortex cores. The mechanisms governing the nonequilibrium vortex-core properties are different well below and close to

T_c.[11] In the strong nonequilibrium close to T_c, vortex cores shrink by a runaway of quasiparticles into the superfluid area,[10] whereas well below T_c they expand due to electron heating to an elevated temperature $T^* > T$.[17] Close to T_c, the transition to the strongly nonequilibrium state is signified by a maximum of $\tilde{I}(V)=I(V)-V/R_n$ at $V_i(I_i) \propto B$,[10] where R_n is the normal-state resistance. For sample G, by approximating $R_n \approx R_0$, the maxima $\langle V_i(I_i)\rangle$ occur at the solid circles in Fig. 4(b), indeed exhibiting $\langle V_i\rangle \propto B$ in support of the vortex-core shrinking being the mechanism behind the nonlinearities in the $\langle V(I)\rangle$. The same numerical procedure for $T=1.1$ K results in the solid circles in Fig. 4(a). These $\langle V_i(I_i)\rangle$ points are weakly dependent on B, which is in agreement with the different nature of the strong nonequilibrium. In spite of $(d\tilde{I}/dV)_{V=V_i}=0$ being not fully justified for finding $\langle V_i(I_i)\rangle$ in this case,[17] the solid circles in Fig. 4(a) are still useful rule-of-thumb pointers to a qualitative change in the vortex-motion dynamics. Other symbols in Fig. 4, i.e., the open circles and triangles, represent $\langle V(I)\rangle$ points that are in connection with the noise and will be defined precisely in Sec. IV A. In sum, above the open circles we observe $\Sigma_V \propto 1/f^{\nu}$, with $\nu=1$ up to the open diamonds and $\nu>1$ beyond.

We complete our analysis of the average dissipation with remarks on a possible flux creep in Nb. In Fig. 4, the $\langle V(I)\rangle$ for $B \to B_{c2}$ and $I \to 50$ μA displays a moderate upturn above $\langle V\rangle = R_0 I$. We cannot rule out that in these conditions a heating in the interface may assist a flux creep in Nb, resulting in a nonlinear increase of the $\langle V\rangle$. However, in the rest of the paper, we concentrate on the noise outside this regime, and the conclusion that the dissipation is produced predominantly by a vortex motion in the a-NbGe in the presence of a spatially modulated J holds.

IV. NOISE

Before turning to details of Σ_V in sample G, we briefly discuss issues which are not central to the paper but should still be commented. Since no voltage dependence of the noise is detected in the normal state, it follows that the interface contributes to S_V negligibly, only by the Johnson-Nyquist noise due to (small) R_{int}. From the measured total noise S_V, Σ_V is calculated as $\Sigma_V = S_V - 4k_B T(d\langle V\rangle/dI)$. Although at $\langle V\rangle > \langle V_i\rangle$ electron heating to $T^* > T$ may take place, the exact temperature is of little relevance. In this regime, we measure $S_V > 10^{-18}$ V^2 s, whereas $d\langle V\rangle/dI \sim 600-700$ Ω in combination with the T_c sets the maximum thermal noise to around 10^{-19} V^2 s. Σ_V below $\langle V_i\rangle$ qualitatively resembles that in Ref. 3. In the presence of pinning, $\Sigma_V(\langle V\rangle)$ is nonmonotonic, being proportional to $\langle V\rangle$ until a maximum is reached and then decreasing as $\langle V\rangle$ grows further. When there is no pining, $\Sigma_V \propto \langle V\rangle^2$ and it is a decreasing function of increasing B, but the scaling $\Sigma_V \propto (1-B/B_{c2})^2\langle V\rangle^2$, found in Ref. 3 for a homogeneous J, is less well defined. We assign this to an already important role of the inhomogeneity of J in the absence of pinning, since ρ is not small.

A. Analysis of the spectra

In our noise measurements, we record $S_V(f)$ averaged in time typically a hundred times. Thus, acquired spectra are then analyzed with regard to phenomena that govern the noise. The highest resolution is obtained by averaging $S_V(f)$ further over Δf, provided S_V does not depend on f, which gives $S_V(\bar{f})$. In a measured spectrum, $S_V(f)$ takes values between some $S_{V,min}$ and $S_{V,max}$, but if the number of recorded points is large enough, the averaging results in an error of $S_V(\bar{f})$ much smaller than $S_{V,max}-S_{V,min}$. In this work, with 400 points between f_1 and f_2, it is possible to resolve $S_V(\bar{f})$ down to 10^{-20} V^2 s even if $S_{V,max}-S_{V,min} \sim 10^{-19}$ V^2 s. The averaging over Δf is not always applicable. It works well if $S_V(f)$ is flat, either by its nature or by its functional dependence that may be such as to result in an apparently constant S_V within $(\bar{f}-\Delta f/2, \bar{f}+\Delta f/2)$. If the averaging is not possible, the accuracy in extracting dependences of S_V on other quantities is reduced. On the other hand, when the f dependence of S_V is simple, a high resolution can be achieved by analyzing the spectra differently. For example, if $S_V \propto 1/f$, it is possible to average fS_V. Sometimes one can also combine $\langle V\rangle$, f, and possibly other variables of interest to merge a number of spectra into a single instructive graph.

Analysis of our $\Sigma_V(f)$ spectra requires a combination of the above approaches. We first note that over a considerable range of the $\langle V(I)\rangle$, between the open circles and triangles in Fig. 4, the spectra exhibit a well defined $\Sigma_V \propto 1/f$ behavior. Within this range, $\Sigma_V \propto \langle V\rangle^2/f$ can appear provided the (T,B) conditions are right and $\langle V\rangle$ is not too close to the open triangles. This is presented in Fig. 5(a) for $T=1.1$ K and $B=1.7$ T, where the spectra from the indicated appreciable span of the $\langle V(I)\rangle$ form a linear curve which extrapolates to zero as $\langle V\rangle \to 0$. The observed $\Sigma_V \propto \langle V\rangle^2/f$ is suggestive of resistance fluctuations, but these plots do not hold over the entire $\langle V(I)\rangle$, so Σ_V as a function of f should be analyzed separately, with $\langle V\rangle$, T, and B as parameters.

The general behavior of $\Sigma_V(f)$, found for all the $\langle V(I)\rangle$ curves in Fig. 4, is demonstrated in Figs. 5(b)–5(d). We again choose $T=1.1$ K and $B=1.7$ T for an easy comparison to $\Sigma_V \propto \langle V\rangle^2/f$ in Fig. 5(a) (see the indicated values of I and $\langle V\rangle$). At low $\langle V\rangle < \langle V_i\rangle$, Σ_V is relatively small and does not display a recognizable f dependence. This is shown in Fig. 5(b), where we plot such a Σ_V (lower curve, left-hand scale) and the corresponding $f\Sigma_V$ (upper curve, right-hand scale) against f. If there is a weak inconstancy of the $\Sigma_V(f)$ in the given f range, it is obscured because the $S_{V,max}-S_{V,min}$ is too large, as seen from not only the $\Sigma_V(f)$ but also the $f\Sigma_V(f)$ being flat. Around $\langle V_i\rangle$, where the vortex dynamics undergoes a change from weak to strong nonequilibrium, for low B the noise magnitude exhibits a steep jump, with the spectra being too distorted to be treated by a simple approach systematically. At larger B, the transition at $\langle V_i\rangle$ is smoothed and no distortion of the spectra is clearly visible even at $\langle V_i\rangle$.

A noticeable $\Sigma_V(f)$ dependence with undistorted spectra is observed when $\langle V\rangle > \langle V_i\rangle$ increases toward the open circles, which are for low B positioned higher because of the wider

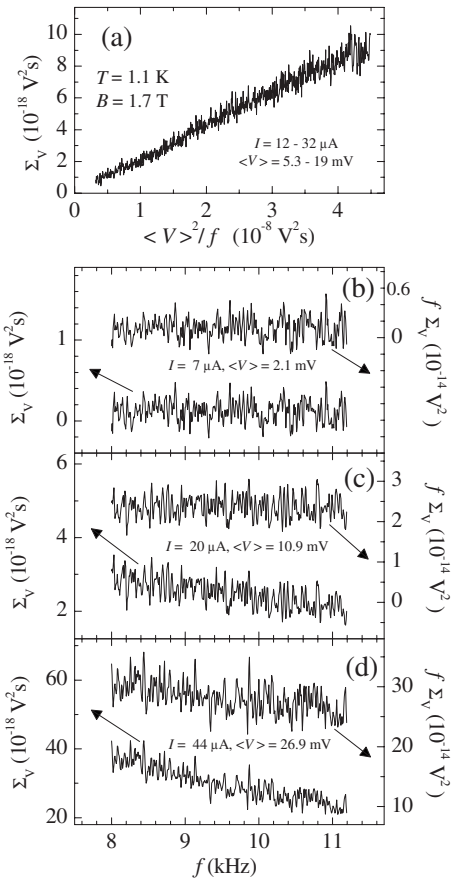

FIG. 5. (a) $\Sigma_V \propto \langle V\rangle^2/f$ for $T=1.1$ K, $B=1.7$ T, and $I=12-32$ μA ($\langle V\rangle=5.3-19$ mV). For the same T and B, in (b)–(d) we plot Σ_V (lower curves, left-hand scales) and $f\Sigma_V$ (upper curves, right-hand scales) against $f_1 \leqslant f \leqslant f_2$. (b) At low $\langle V\rangle$, both $\Sigma_V(f)$ and $f\Sigma_V(f)$ are flat; the noise is too small to extract the f dependence of Σ_V. As $\langle V\rangle$ increases, $\Sigma_V(f) \propto 1/f^{\nu}$ can be resolved clearly, with (c) $\nu=1$ in a range of $\langle V\rangle$ and (d) $\nu>1$ at larger $\langle V\rangle$.

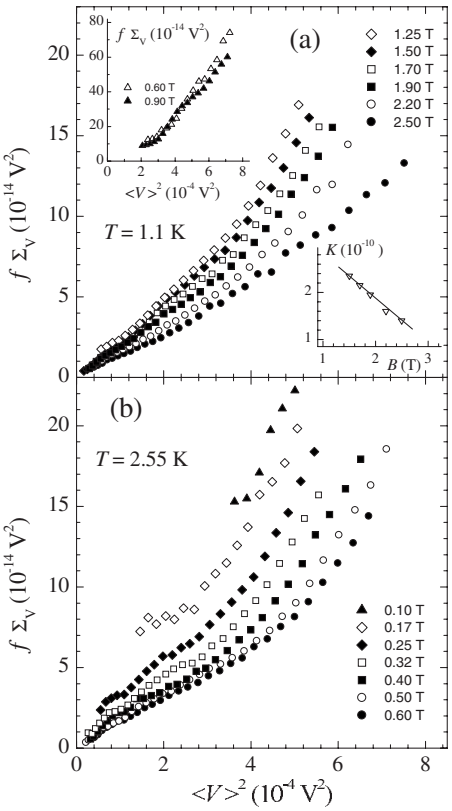

FIG. 6. Averaged $f\Sigma_V$ vs $\langle V\rangle^2$ for the spectra of the type shown in Fig. 5(c). Irrespective of T, the noise decreases with increasing B. (a) $T=1.1$ K. At $B=0.6$ and 0.9 T, the noise is considerably larger than at higher B, and it is shown in the upper inset. For $B \geqslant 1.5$ T, the low-$\langle V\rangle$ part can be approximated by a linear dependence, with a slope K plotted against B by the symbols in the lower inset and the solid line indicating $K \propto 1/B$. (b) $T=2.55$ K. $f\Sigma_V \propto \langle V\rangle^2$ at low $\langle V\rangle$ is acceptably well defined only for $B=0.5$ and 0.6 T.

transition region around $\langle V_i\rangle$. In this regime, the noise is $\Sigma_V \propto 1/f^{\nu}$, in particular, with $\nu=1$ between the open circles and open triangles, as exemplified in Fig. 5(c). The Σ_V decreases with increasing f, while the $f\Sigma_V$ is flat. This clarifies the criterion in determining the open circles in Fig. 4. They correspond to the first $\langle V(I)\rangle$ points where, beyond doubt, the Σ_V does and the $f\Sigma_V$ does not depend on f. When $\langle V\rangle$ exceeds the open triangles, ν increases above unity but remains well below 2, as visible in Fig. 5(d), where both the Σ_V and $f\Sigma_V$ decrease with increasing f.

The above consideration reveals how the frequency dependence of Σ_V changes upon increasing $\langle V\rangle$. In particular, $\Sigma_V \propto 1/f^{\nu}$ is observed in essentially the same range of the $\langle V(I)\rangle$ where a strong modulation of the J takes place, which will be discussed further in Sec. V.

B. $\langle V\rangle$, T, and B properties of the noise

Σ_V increases monotonically with increasing $\langle V\rangle$ always, except for $\langle V\rangle \ll \langle V_i\rangle$ in the presence of pinning at low T, as mentioned before. We skip the nonmonotonic Σ_V vs $\langle V\rangle$, described in detail in Ref. 3, in order to pay attention to $\Sigma_V \propto 1/f^{\nu}$ at larger $\langle V\rangle$. Since ν changes along the $\langle V(I)\rangle$, for brevity we focus on $\nu=1$, which covers a substantial portion of the $\langle V(I)\rangle$ for both characteristic temperatures and, hence, captures the main physics of Σ_V. We, therefore, average these flat $f\Sigma_V(f)$ spectra to obtain essential information on Σ_V as a function of $\langle V\rangle$, T, and B. This results in $f\Sigma_V$ vs $\langle V\rangle^2$ plots in Fig. 6 for (a) $T=1.1$ K and (b) $T=2.55$ K. At both temperatures, Σ_V decreases as B increases.[23] The $\Sigma_V(B)$ dependence at 2.55 K is smooth over the whole range $0.15 \lesssim B/B_{c2} \lesssim 0.85$ of our measurements, and at 1.1 K for $0.4 \lesssim B/B_{c2} \lesssim 0.8$. At the latter temperature, Σ_V increases steeply at lower B/B_{c2} and the corresponding curves ($B=0.6$ and 0.9 T) are displayed in the upper inset of Fig. 6(a) for clarity.

$f\Sigma_V$ is approximately linear in $\langle V\rangle^2$, with $\Sigma_V \to 0$ as $\langle V\rangle$ is extrapolated to zero, only for some curves at $\langle V\rangle^2$ below $\sim 3\times 10^{-4}$ V^2. In our measurements, this applies to 1.5 T $\leqslant B \leqslant$ 2.5 T at $T=1.1$ K, and to 0.5 T $\leqslant B \leqslant$ 0.6 T at $T=2.55$ K. We use the relatively wide B range of the above approximation at 1.1 K to address the noise magnitude phenomenologically. The slope $K=f\Sigma_V/\langle V\rangle^2$ for these data is shown as a function of B in the lower inset of Fig. 6(a) by the symbols, whereas the solid line indicates $K=(3.3$

$\times 10^{-10}$ T)/B. Since the number of vortices in the sample is $N_\phi \approx n_\phi lw$, where $n_\phi = B/\phi_0$ is the vortex density, the $K(B)$ complies with the Hooge expression[6] which states that K is inversely proportional to the number of fluctuators. In the Hooge approach, $K = \alpha_H / N_\phi$, and the Hooge constant α_H is in our case around 4×10^{-5}. Although it has been widely accepted that the Hooge formula is of a descriptive value only,[15] α_H is still frequently used as a measure of the magnitude of $1/f$ noise. The obtained α_H is much smaller than that in Ref. 5 for Au films, namely, $\sim 2 \times 10^{-3}$ traditionally taken as a reference, implying that in our experiment we deal with a relatively quiet system.

At large $\langle V \rangle$, the noise is not linear in $\langle V \rangle^2$ and exhibits a stronger dependence for all the data in Fig. 6. In general, $\Sigma_V \propto \langle V \rangle^2$ is straightforward only for Ohmic resistors with a voltage-independent resistance fluctuation $(\delta R)^2$. In this case, if a fluctuating resistor is biased by a constant I, the voltage fluctuation is $(\delta V)^2 = [(\delta R)^2/R^2]V^2 \propto V^2$. For a nonlinear $\langle V(I) \rangle$, a separate consideration in each particular case is required, as it was, for example, done for Josephson tunnel junctions.[24]

V. DISCUSSION

The measured average voltage and noise arise from the integrated longitudinal component $E_x(\mathbf{r}) = \phi_0 n_\phi(\mathbf{r}) u_y(\mathbf{r})$ of the spatially varying electric field and its time (t) dependent fluctuation $\delta E_x(\mathbf{r}, t)$, where $\mathbf{r}$ is the in-plane coordinate and u_y the transversal component of the vortex velocity. The compression modulus C_{11} of a vortex system is large, thus $n_\phi(\mathbf{r}) \approx B/\phi_0 = n_\phi$ and $E_x(\mathbf{r}) \approx \phi_0 n_\phi u_y(\mathbf{r})$. A strong $\mathbf{u}(\mathbf{r})$ dependence is allowed by the small shear-stress modulus C_{66} in a-NbGe.[20] The nonuniform $\mathbf{J}$ produces an inhomogeneous vortex motion according to $\phi_0 \mathbf{J}(\mathbf{r}) \times \hat{\mathbf{z}} = \eta \mathbf{u}(\mathbf{r})$, where the viscosity coefficient η accounts for the mechanisms of the power dissipation and a small term related to the inertial vortex mass[12] has been disregarded. The variation of $J(\mathbf{r})$ over the sample in the regime where $\Sigma_V \propto 1/f^\nu$ is such that weak and strong nonequilibria are present simultaneously. This situation is difficult to treat in a fully quantitative manner, but we can use findings of Refs. 3, 11, 12, and 20 for the same material in the presence of a homogeneous or a weakly modulated J to elucidate the cause and structure of Σ_V. We start by addressing the f dependence of Σ_V, which shows a certain generality, and later discuss the noise as a function of $\langle V \rangle$, T, and B, where the nature of the strong nonequilibrium is more important. For simplicity, scalar notation for $\mathbf{E}$, $\mathbf{J}$, and $\mathbf{u}$ is used.

δE is a random process with a characteristic time τ. This leads to $[\delta V(t)]^2 \propto [\delta E(t)]^2 \propto \exp(-t/\tau)$ and a DL spectrum $\Sigma_V \propto \tau/[1+(\omega\tau)^2]$, where $\omega = 2\pi f$. If the physics of a system changes with E, which is, thus, more than an unperturbing response to J, then each E-dependent state has a different τ. A range of E results in $\tau_1 \leqslant \tau \leqslant \tau_2$ and Σ_V is altered by a distribution $D(\tau)$ of the characteristic times, i.e., $\Sigma_V \propto \int \tau D(\tau)[1+(\omega\tau)^2]^{-1} d\tau$ from τ_1 to τ_2.[16] A power-law-like $\Sigma_V(f)$ is obtained with $D \propto \tau^{-q}$,

$$\Sigma_V \propto \frac{1}{f^{2-q}} \int_{\omega\tau_1}^{\omega\tau_2} \frac{x^{1-q} dx}{1+x^2} = \frac{1}{f^{2-q}} Z_q(\omega, \tau_1, \tau_2). \quad (1)$$

In particular, $Z_1 = \arctan(\omega\tau_2) - \arctan(\omega\tau_1)$ depends on f weakly if $\tau_2^{-1} \ll \omega \ll \tau_1^{-1}$, and under these circumstances, $\Sigma_V \propto 1/f$ holds well. For other values of $0 < q < 2$, the Z_q correction to the power law $\Sigma \propto 1/f^\nu$ is also weak if τ satisfies the above condition; therefore, $\Sigma_V \propto 1/f^\nu$ with $0 < \nu < 2$ agrees with the model if a wide spread in τ is characteristic of the system. This approach has been widely used in explaining $1/f$ type of noise not only in the conduction of normal electrons[15,16] but also in vortex-motion-generated dissipation.[3,13,14] However, in the latter studies, the arguments in favor of a distribution of τ relied on somewhat heuristic assumptions, such as the presence of vortex bundles[13] or of a mixture of depinned solid and "liquid" vortex phases.[3,14] In our case, a range of τ follows straightforwardly from a coexistence of distinct E-dependent vortex states.

We recall the result of Sec. IV A that the development of $\Sigma_V \propto 1/f^\nu$ as $\langle V \rangle$ increases is similar close to and well below T_c, although the strongly nonequilibrium regimes, where these spectra appear, are physically different (see Sec. III B). The spatial variation of vortex states can be parametrized through that of the vortex-core area $A_c \sim \xi^2 \pi$. For low J, i.e., far away from the interruption in the Nb line, A_c has essentially the equilibrium value determined by T only. As J (and E) increases toward the central region of the microbridge, the vortices gradually undergo changes because the nonequilibrium dynamics takes place, i.e., $A_c(T) \rightarrow A_c(T, E)$. A continuous variation of $A_c(T, E)$ over the sample implies a continuous range of τ if δE is interrelated with the VCFS δA_c, and this holds because the mixed-state dissipation depends strongly on the size of vortex cores.

The above picture in connection with Eq. (1) explains the appearance of $\Sigma_V \propto 1/f^\nu$ solely by ascribing a wide range of τ to the simultaneous presence of qualitatively different vortices. The inhomogeneity of the fluctuations, crucial for the theory, in our experiment emerges as a consequence of the geometry of our hybrid sample and the strong sensitivity of vortex properties in a-NbGe to a moderate E. Moreover, the high-dissipation regime of our $\Sigma_V \propto 1/f^\nu$ spectra depends little on sample-dependent structural disorder (sets pinning potential) or thermodynamics of the mixed state (solid vs liquid). This is a consequence of the strong domination of the processes pertaining to fundamental parameters of type II superconductivity.[10,11,17] In turn, the application of Eq. (1) to our results does not require suppositions on material-dependent properties.

Now we turn to the noise magnitude, discussing first briefly the relationship between Σ_V and δA_c. In Ref. 3, it was shown that Σ_V for a homogeneous, weakly nonequilibrium flux flow with Ohmic $\langle V(I) \rangle$ was linked to the VCSF's by $\Sigma_V / \langle V \rangle^2 \propto (\delta A_c)^2 / A_c^2$. The origin of δA_c was in thermal fluctuations of the quasiparticle density, leading to the fluctuations of the "pressure" that stabilized the vortex-core boundary. $\delta A_c / A_c$ was independent of $\langle V \rangle$ and this resulted in $\Sigma_V \propto \langle V \rangle^2$, while the application of the LO theory to the $\Sigma_V(B)$

led to a conclusion that δA_c was proportional to the area per vortex.

This model can be extended to the current situation. If A_c is determined by a quasiparticle distribution that depends explicitly on temperature $T^* \geqslant T$ only, then $E=\rho_n n_\phi J A_c(T^*)$, where $A_c(T^*)=A_c(T,E)$ is set by the equilibrium (T) and the departure (E) from it, linked to $T^*(E)$. When A_c depends on E explicitly, i.e., for the LO mechanism, the proper expression is $E=\rho_n n_\phi J A_c^2(T,0)/A_c(T,E)$.[10] In strong nonequilibrium, the leading term in δE originates in $\delta A_c(T,E)$, and a convenient expression applicable to both cases is

$$\frac{\Sigma_V}{\langle V\rangle^2} \propto \frac{\langle(\delta E)^2\rangle}{\langle E\rangle^2} \propto \frac{\langle[\delta A_c(T,E)]^2\rangle}{\langle A_c(T,E)\rangle^2}. \tag{2}$$

For a collective of vortices, the above single-vortex approach is corrected with respect to particular T/T_c and B/B_{c2} conditions,[3,10] which can, however, be treated more manageably by *ad hoc* inclusions of findings of Refs. 3 and 11. Despite these simplifications and the intricacy of spatial averaging, the basic concepts remain the same and Eq. (2) represents an ample groundwork for analyzing our results further.

At $T \ll T_c$, the strong nonequilibrium corresponds to a thermal-like quasiparticle distribution with $T \to T^*$.[11,17] Since the distribution remains of the same form as in equilibrium, $A_c(T^*)$ is governed by the reduction $B_{c2}(T) \to B_{c2}(T^*)$ only. It follows that $A_c(T^*)/A_c(T)=B_{c2}(T)/B_{c2}(T^*)$, therefore vortex cores expand. This process is interrelated with E through the $T^*(E)$ dependence, determined in Ref. 11 for a homogeneous J and several $B/B_{c2}(T)$ at the same $T=1.1$ K as used here. The assumption of a spatially dependent $A_c(T,E)$ requires a nonuniform T^*, the hottest being around the interruption in the Nb line where E is the largest. Temperature variations over microbridge films in the presence of a strongly nonequilibrium vortex motion at $T \ll T_c$ were reported,[25] which supports this point of view. It is reasonable to assume that T^* has a fluctuation δT^*, similarly as in Ref. 8, where this caused resistance fluctuations $\propto \langle V\rangle^2/f$ in normally conducting, Ohmic thin films. The simple relationship between A_c and B_{c2} allows us to convert Eq. (2) into a form more suitable for discussing the results in Fig. 6(a). $A_c \propto 1/B_{c2}$ leads to $(\delta A_c/A_c)_{T=T^*}=-[(dB_{c2}/dT)/B_{c2}]_{T=T^*}\delta T^*$. Without introducing a significant error, we can approximate $B_{c2}(T)=B_{c2}(0) \times (1-T/T_c)$ to obtain

$$\frac{\Sigma_V}{\langle V\rangle^2} \propto \frac{\langle(\delta T^*)^2\rangle}{\langle(T_c - T^*)^2\rangle}. \tag{3}$$

Although the $\langle[\delta T^*(B)]^2\rangle$ dependence certainly impacts the noise, the $\Sigma_V(B)$ in Fig. 6(a) is dominated by the denominator of Eq. (3), as it can vary strongly: between $(T_c-T)^2$ and zero in the limits $B \to B_{c2}(T)$ and $B \to 0$, respectively. T^* for the same E is smaller at larger B,[11] hence the denominator increases with increasing B and diminishes Σ_V accordingly. The remarkable steep enhancement of the $\Sigma_V(B)$ at low B [displayed in the upper inset of Fig. 6(a)] can also be understood in terms of Eq. (3) by its diverging form as T^* increases toward T_c for low vortex density. Moreover, $\Sigma_V \propto \langle V\rangle^2$ at high B and not too large $\langle V\rangle$ implies a relative constancy of the right-hand side of Eq. (3). This is plausible because the denominator is reduced to not much below $(T_c - T)^2$, and $(\delta T^*)^2$ should not depend on E strongly when the departure from the equilibrium is moderate.

Close to T_c, the nonequilibrium quasiparticle distribution function is not thermallike and A_c is not determined by B_{c2} only. Vortex cores shrink according to $A_c(T,E) =A_c(T,0)/[1+(E/E_i)^2]$, which can proceed down to $A_{c,min}(T)=A_c(T,0)\sqrt{1-T/T_c}$.[10] Here, $E_i=u_i B$ is a characteristic electric field set by a B-independent vortex velocity $u_i \propto \sqrt{(1-T/T_c)^{1/2}/\tau_{in}}$, where τ_{in} is the inelastic electron-phonon scattering time. Core shrinking requires a density of thermal phonons sufficient to enable an efficient heat transfer from electrons to the bath, which was shown to be the case for a-NbGe microbridges at $T \approx 2.5$ K.[11] Consequently, the results in Fig. 6(b) refer to a uniform temperature $\tilde{T} \gtrsim T$ over the sample and vortices which can vary in size between $A_{c,min}(\tilde{T})$ and $A_c(\tilde{T},0)$. The situation is equivalent to that at $T \ll T_c$ in the sense of a coexistence of nearly equilibrium vortices far away from the interruption in the Nb line and nonequilibrium ones (smaller in this case) around it, which explains the similarity in the development of $\Sigma_V \propto 1/f^\nu$ spectra. As seen in Fig. 6(b), the decrease of the $\Sigma_V(B)$ with increasing B is again present, whereas the nonlinearity of the Σ_V vs $\langle V\rangle^2$ dependence is not much stronger than at $T=1.1$ K, especially when B approaches $B_{c2}(T)$. However, in contrast to the $T \ll T_c$ behavior, the noise below $B \sim 0.3B_{c2}(T)$ does not grow steeply, but instead continues with the smooth increase as B is lowered.

The heating $T \to \tilde{T}$, theoretical details of which are given in Ref. 18, in similar $a-$NbGe films under basically the same conditions as here was found to be weak, i.e., it did not leave a measurable signature in the $\langle V(I)\rangle$.[11] The noise is, however, sensitive to the fluctuation $\delta\tilde{T}$, resulting in δA_c. The main contribution to Σ_V given by Eq. (2) is expected to arise from the E-dependent term in $A_c(T,E)$ through the temperature dependence of u_i (i.e., E_i). Hence, $\delta A_c \approx [(\partial A_c/\partial u_i) \times (\partial u_i/\partial T\,]_{T=\tilde{T}}\delta\tilde{T}$. In the limit $u \gg u_i$ of strong equilibrium, which is of main interest here, $\delta A_c/A_c \sim [(\partial u_i/\partial T)/u_i]_{T=\tilde{T}}\delta\tilde{T}$. Since the T dependence of u_i is dominated by $(1-T/T_c)^{1/4}$, from Eq. (2) we obtain

$$\frac{\Sigma_V}{\langle V\rangle^2} \propto \frac{\langle(\delta\tilde{T})^2\rangle}{\langle(T_c - \tilde{T})^2\rangle}. \tag{4}$$

An additional small contribution due to $\delta A_c(\tilde{T},0)$ follows the above expression as well, since the principles used in deriving Eq. (3) apply. Therefore, Eq. (4) provides an adequate form for discussing the noise close to T_c.

Although Eq. (4) appears analogous to Eq. (3), its implications are different. In Ref. 18, it was argued that $\tilde{T}$ increases with increasing B, proportionally to B at $B \ll 0.4B_{c2}$ and saturating at higher B, but stays below T_c. This heating, therefore, does not lead to a transition to the normal state. Since $\tilde{T}-T$ is small, the denominator in Eq. (4) remains of

the order of $(T_c-T)^2$ and there is no tendency of Σ_V to diverge at any B. This explains the main difference between $\Sigma_V(B)$ at the two temperatures. With a fairly constant $T_c-\tilde{T}$, the noise depends on B mainly through $\langle[\delta\tilde{T}(B)]^2\rangle$, which should decrease as vortex density increases and $\tilde{T}(B)$ stabilizes at the saturation value. In the $\tilde{T}$-saturating, high-B regime (and provided $\langle V\rangle$ is not too large, see below), the right-hand side of Eq. (4) is approximately constant and $\Sigma_V \propto \langle V\rangle^2$, complying with the observation.

Regarding the nonlinear Σ_V vs $\langle V\rangle^2$, at large $\langle V\rangle$, found for both characteristic regimes, it can be explained as a consequence of an increase of the right-hand side of Eq. (2) when nonequilibrium becomes very strong. Obviously, a detailed quantitative description of this behavior extends beyond the simplifications used in understanding the physics behind our results.

VI. SUMMARY AND CONCLUSIONS

A hybrid *a*-NbGe/Nb structure is probed experimentally in order to study some general aspects of $1/f$ noise as well as specific fluctuations related to vortices in motion. A weak-pinning *a*-NbGe microbridge is used as a medium for vortex motion. On top of the microbridge, a strong-pinning, longitudinal Nb line with a narrow interruption in the middle is added. The applied current, coming from the *a*-NbGe contact pads, at the entry to the microbridge, splits into two branches and a part of it flows through Nb. Since at the interruption the current returns to the *a*-NbGe fully, a modulation of the current density J within the *a*-NbGe appears. As the *a*-NbGe is becoming more dissipative, the modulation strengthens, which has a strong influence on the mixed state therein. The conditions over the sample are, thus, varying to produce a range of coexisting vortex states, defined by the (local) properties of the distribution function for normal excitations in the cores. The vortices preserve their equilibrium properties in parts of the sample where J is low, but elsewhere they are subject to changes due to a strong nonequilibrium set by the high J. The simultaneous presence of qualitatively distinct vortices results in the noise power spectrum being proportional to $1/f^{\nu}$, with a significant range of $\nu=1$. This can be explained by a statistical integration of Debye-Lorentz spectra over a range of characteristic times, which in our experiment has a direct connection with the spatial variation of the quasiparticle excitation spectrum. The appearance of the $1/f^{\nu}$ noise is similar for temperatures well below and close to T_c, although the corresponding nonequilibrium vortex properties are different. The noise magnitude is more sensitive to details of the strong nonequilibrium, but the mechanism underlying the noise is the same: dynamic fluctuations of the vortex-core size. With this model, we can account for the main features of the noise in both characteristic regimes, i.e., at low temperatures, where vortices expand due to electron heating, and close to T_c, where vortices shrink due to the Larkin-Ovchinnikov mechanism.

ACKNOWLEDGMENTS

This work has been supported by the DFG within GRK 638 and SFB 631, as well as by the MZOS 119-1191458-1008.

*Corresponding author; dbabic@phy.hr
†Present address: Siemens VDO Automotive AG, Siemensstrasse 12, D-93055 Regensburg, Germany.

[1] M. Henny, S. Oberholzer, C. Strunk, and C. Schönenberger, Phys. Rev. B **59**, 2871 (1999).
[2] D. J. van Ooijen and G. J. van Gurp, Phys. Lett. **17**, 230 (1965); G. J. van Gurp, Phys. Rev. **166**, 436 (1968).
[3] D. Babić, T. Nussbaumer, C. Strunk, C. Schönenberger, and C. Sürgers, Phys. Rev. B **66**, 014537 (2002).
[4] For a direct experimental evidence, see D. Babić, in *New Frontiers in Superconductivity Research*, edited by B. S. Martins (Nova Science, New York, 2006).
[5] F. N. Hooge and A. M. H. Hoppenbrouwers, Physica (Utrecht) **45**, 386 (1969).
[6] F. N. Hooge, Phys. Lett. **29**, 139 (1969).
[7] J. Clarke and R. F. Voss, Phys. Rev. Lett. **33**, 24 (1974).
[8] R. F. Voss and J. Clarke, Phys. Rev. B **13**, 556 (1976).
[9] J. H. Scofield, J. V. Mantese and W. W. Webb, Phys. Rev. B **32**, 736 (1985).
[10] A. I. Larkin and Yu. N. Ovchinnikov, in *Nonequilibrium Superconductivity*, edited by D. N. Lengenberg and A. I. Larkin (North Holland, Amsterdam, 1986).
[11] D. Babić, J. Bentner, C. Sürgers, and C. Strunk, Phys. Rev. B **69**, 092510 (2004).
[12] D. Babić, J. Bentner, C. Sürgers, and C. Strunk, Physica C **432**, 233 (2005).
[13] W. J. Yeh and Y. H. Kao, Phys. Rev. B **44**, 360 (1991).
[14] P. J. M. Wöltgens, C. Dekker, S. W. A. Gielkens, and H. W. de Wijn, Physica C **247**, 67 (1995).
[15] M. B. Weissman, Rev. Mod. Phys. **60**, 537 (1988).
[16] P. Dutta and P. M. Horn, Rev. Mod. Phys. **53**, 497 (1981).
[17] M. N. Kunchur, Phys. Rev. Lett. **89**, 137005 (2002).
[18] A. I. Bezuglyj and V. A. Shklovskij, Physica C **202**, 234 (1992).
[19] A. Helzel, I. Kokanović, D. Babić, L. V. Litvin, F. Rohlfing, F. Otto, C. Sürgers, and C. Strunk, Phys. Rev. B **74**, 220510(R) (2006).
[20] J. Bentner, D. Babić, C. Sürgers, and C. Strunk, Phys. Rev. B **70**, 184516 (2004).
[21] C. Peroz and C. Villard, Phys. Rev. B **72**, 014515 (2005).
[22] A highly resistive interface was made by depositing a thin Ge layer between the *a*-NbGe and Nb.
[23] The spectra with $\nu>1$ continue this trend.
[24] J. Clarke and G. Hawkins, Phys. Rev. B **14**, 2826 (1976).
[25] Z. L. Xiao, E. Y. Andrei, and P. Ziemann, Phys. Rev. B **58**, 11185 (1998).